Langmuir
Article
pubs.acs.org/Langmuir
© XXXX American Chemical Society

Laplace Barriers for Electrowetting Thresholding and Virtual Fluid Confinement

E. Kreit,[†] M. Dhindsa,[†] S. Yang,[†] M. Hagedon,[†] K. Zhou,[§] I. Papautsky,[‡] and J. Heikenfeld*[,†]

[†]*Novel Devices Laboratory, and* [‡]*BioMicroSystems Laboratory, School of Electronics and Computing Systems, University of Cincinnati, Cincinnati, Ohio 45221, United States, and* [§]*Gamma Dynamics Corp., Cincinnati, Ohio 45219, United States*

Received July 1, 2010

Reported are Laplace barriers consisting of arrayed posts or ridges that impart ~100 to 1000 s of N/m^2 Laplace pressure for fluid confinement, but the Laplace pressure is also small enough such that the barriers are porous to electrowetting control. As a result, the barriers are able to provide electrowetting flow thresholding and virtual fluid confinement in noncircular fluid geometries. A simple theoretical model for the barriers and experimental demonstrations validate functionality that may be useful for lab-on-chip, display devices, and passive matrix control, to name a few applications.

Introduction

Microfluidics is dominated by the use of fixed geometry channels to confine and direct fluids.[1] However, there are also numerous techniques for creating programmable microfluidics where the user can select two or more fluid pathways. Theoretically, the most desirable programmable approach is to use "virtual" confinement (no physical walls). With proper stimulus to control the fluid flow and geometry, virtual confinement maximizes the accessible number of fluid networks, geometries, and flow vectors. It is well known that programmable and virtual confinement can be achieved by applying electrical fields, including DC or low-frequency voltage for electrowetting[2,3] and high-frequency voltage for dielectrophoresis.[4] However, traditionally, the electrical stimulus must be maintained to hold the channel geometry, or else the fluid will return to a geometry that minimizes its surface area (Figure 1a).

Recently, we reported a novel technique for creating virtual electrowetting channels.[5] In this approach, fluid propagation through an array of posts is enabled as fluid wets against a next set of posts and is a more-applied subset of theoretical work by Yeomans et al. on Gibbs' pinning.[6] Importantly, when the voltage was removed, the fluid confinement persisted and could be altered only by another application of an electrical stimulus. At the end of our first report,[5] we stated the need for simplified fabrication and operation because the electrowetting contact angle modulation was near the practical limit (near contact angle saturation). Furthermore, in our first report, the effect of capillary fingering was theoretically unresolved and experimentally unavoidable.

We demonstrate herein our second generation approach that we refer to as Laplace barriers. Laplace barriers can be easily adapted to any conventional electrowetting microchannel device but enhance device function by virtually confining the fluid in any geometry even without the application of voltage (Figure 1b,c). Unlike our first report where electrowetting to a contact angle of ~45° was required,[5] Laplace barriers require electrowetting contact angle modulation down to only ~90°, or even greater with proper design of the Laplace barrier. The Laplace barriers are constructed of arrayed posts or ridges that impart Laplace pressure to confine the fluid, but the Laplace pressure is also small enough such that the barriers are porous to electrowetting control. Using posts in air or ridges in air or oil, this second-generation approach is also able to operate without capillary fingering. Unlike using contact angle hysteresis for fluid stabilization, Laplace barriers allow fluid advancement without the loss of Laplace pressure at the receding end of a fluid and therefore with greater fluid flow rate. Laplace barriers can be modeled using simple Laplace theory coupled to electrowetting contact angle or other fluid transport forces. These Laplace barriers are theoretically free from the need to consider Gibbs' pinning[6] because Young's angle (θ_Y) is always ~180° on the surfaces of the Laplace barriers. Otherwise, the use of the term "Laplace barrier" would be incorrect. The Laplace barriers reported herein possess the same potential benefits that we previously described for lab-on-chip[5] and also have expanded utility specific to displays[7,8] or robust passive-matrix[9] electrical addressing.

Design Criteria for Laplace Barriers

The selection of the Laplace barrier systems tested herein was motivated by two major requirements. The first goal: above a certain threshold, the Laplace barrier should allow electrowetting control similar to that achieved in a planar open channel (between two plates). The second goal: with electrowetting stimulus below a certain threshold, the Laplace barrier system should maintain the fluid geometry imparted by electrowetting. There are several techniques to create a Laplace barrier. One could attempt to realize this function by utilizing surface energy patterning (i.e., having

*Corresponding author. Tel: 513-556-4763. Fax: 513-556-7326. E-mail: heikenjc@ucmail.uc.edu.

(1) Whitesides, G. M. *Nature* **2006**, *442*, 368–373.
(2) Mugele, F.; Klingner, A.; Buehrle, J.; Steinhauser, D.; Herminghaus, S. *J. Phys.: Condens. Matter* **2005**, *17*, S559–S576.
(3) Baret, J.; Decre, M.; Herminghaus, S.; Seemann, R. *Langmuir* **2003**, *19*, 7646–7651.
(4) Jones, T. B.; Gunji, M.; Washizu, M.; Feldman, M. J. *J. Appl. Phys.* **2001**, *89*, 1441–1448.
(5) Dhindsa, M.; Heikenfeld, J.; Kwon, S.; Park, J.; Rack, P. D.; Papautsky, I. *Lab Chip* **2010**, *10*, 832–836.
(6) Blow, M. L.; Kusumaatmaja, H.; Yeomans, J. M. *J. Phys.: Condens. Matter* **2009**, *21*, 464125.
(7) Heikenfeld, J.; Zhou, K.; Kreit, E.; Raj, B.; Yang, S.; Sun, B. *Nat. Photonics* **2009**, *3*, 292–296.
(8) Blankenback, K.; Schmoll, A.; Bitman, A; Bartels, F.; Jerosch, D. *J. Soc. Inf. Disp.* **2008**, *16*, 237–244.
(9) Abolhasani, M. *Enhanced Addressability and Localization in Digital Microfluidic Multiplexer Systems*. M.S. Thesis, Sharif University of Technology, Iran, April 2010.

 DOI: 10.1021/la104090t

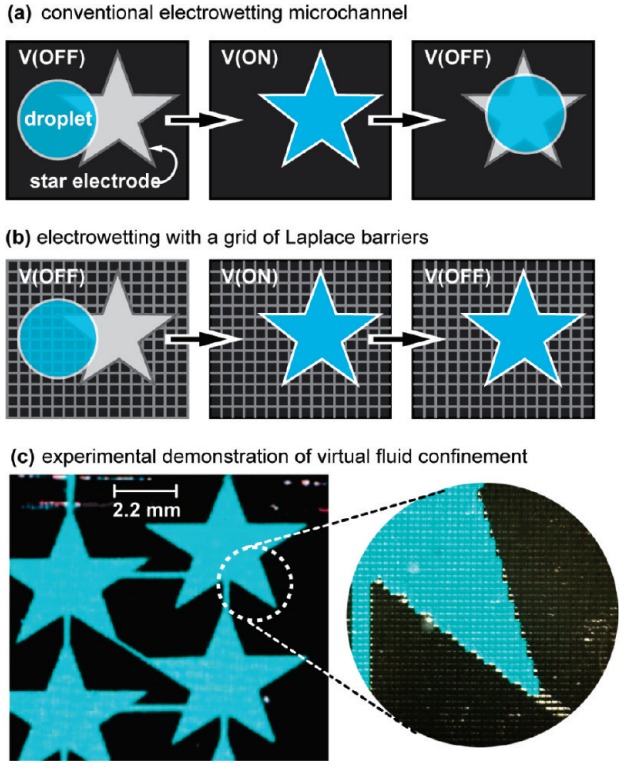


Figure 1. Top view of electrowetting between two plates (microchannel): (a) conventional behavior, (b) behavior with Laplace barriers, and (c) experimental demonstration of a Laplace barrier illustrating tight geometrical confinement. The blue color is the water phase surrounded by a transparent oil.

well-defined regions with greater hydrophobicity). Similarly, one might pattern voids in a substrate, which effectively increases the average hydrophobicity encountered by an advancing fluid.[10] Simply using contact angle hysteresis is not an option; hysteresis reduces the receding end contact angle for a droplet, causing lower Laplace pressure and slower fluid transport. In this work, we use two distinct approaches to periodically alter the channel dimensions and impart greater Laplace pressure on a fluid as it attempts to advance. The first Laplace barrier structure reported herein consists of post arrays similar to those previously reported.[5] However, the post arrays demonstrated herein are not capable of electrowetting, and the mechanism for fluid propagation is unique. The posts simply impart a decrease in the meniscus radius of curvature in the horizontal plane and therefore a localized increase in Laplace pressure. The second Laplace barrier structure uses an array of ridges. The ridges also promote a localized increase in Laplace pressure, but the radius of curvature is decreased in the vertical plane. In terms of fluids to be tested, a conducting fluid (water) was tested in the presence of air and oil. Oil is preferred over air because it: (1) promotes a Young's angle (θ_Y) of ~180°, which eliminates Gibbs' pinning from the theoretical and experimental results; (2) simplifies the predictive calculations for Laplace pressure; and (3) reduces hysteresis and gravity/vibration effects. A simple model for each Laplace barrier structure will now be presented.

Model for the Horizontal Laplace Barriers (Post Arrays)

The Laplace barrier systems rely on a competition between Laplace and electromechanical (electrowetting) pressure. Laplace

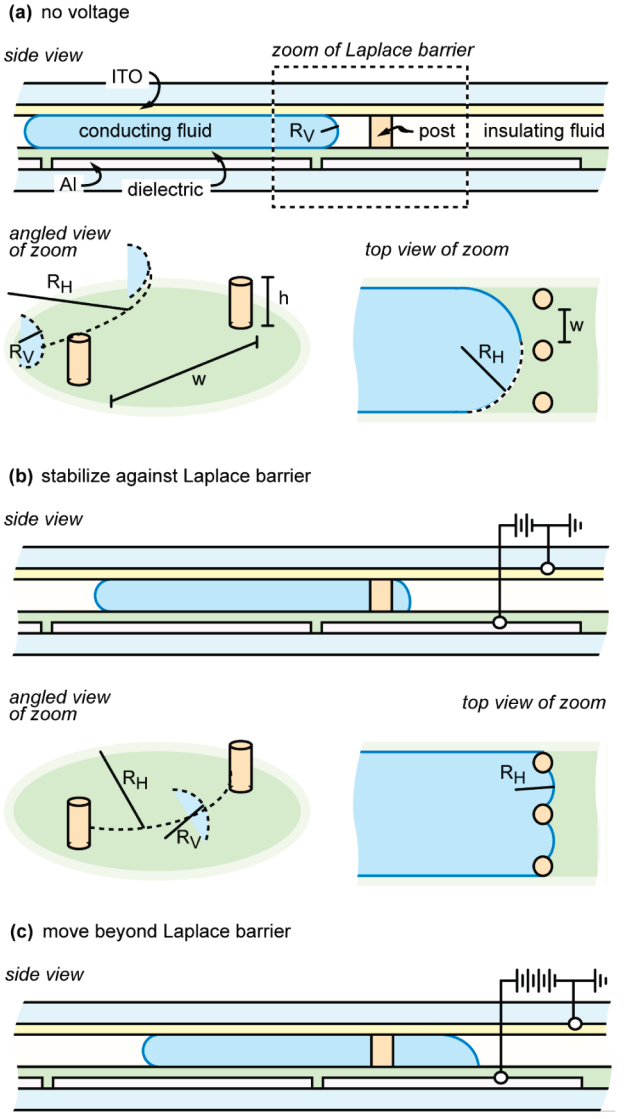


Figure 2. Diagram of a horizontal Laplace barrier created by an array of posts: (a) example construction; (b) stabilizing polar fluid against the Laplace barrier; and (c) advancing polar fluid beyond the Laplace barrier. All device features are coated with a very thin (50 nm) and hydrophobic fluoropolymer.

pressure[11] can be calculated as follows

$$\Delta p = \gamma_{ci}(1/R_1 + 1/R_2) \quad (1)$$

which includes interfacial surface tension between the conducting and insulating fluids (γ_{ci}) and the principle radii of curvature for the conducting fluid meniscus (R_1, R_2). With reference to Figure 2, the radii of curvature are dependent on the conducting fluid's contact angle. For the case of confinement between top (T) and bottom (B) plates separated by a channel height (h), R can be calculated as

$$R = -h/(\cos\theta_T + \cos\theta_B) \quad (2)$$

Next, the effect of electrowetting[2] must be included in the model. The bottom plate includes a thicker and electrically insulating hydrophobic dielectric. Therefore, the bottom plate

(10) Heikenfeld, J.; Dhindsa, M. *J. Adhes. Sci. Technol.* **2008**, *22*, 319–334.

(11) Berthier, J. *Microdrops and Digital Microfluidics*; William Andrew: Norwich, NY, 2008.

is capable of electrowetting modulation

$$\cos\theta_B = \frac{\gamma_{id} - \gamma_{cd}}{\gamma_{ci}} + \frac{C \cdot V^2}{2\gamma_{ci}} \quad (3)$$

where C is the capacitance per unit area of the hydrophobic dielectric and V is the applied DC voltage or AC rms voltage. Typically, contact angle modulation of conducting aqueous fluids in insulating oil ranges from 180 to ~60−45°, beyond which the contact angle modulation ceases because of contact angle saturation.[2] It should be emphasized that electrowetting is an electromechanical effect,[12] and eqs 1−3 can also be used to derive an electromechanical pressure in the channel directly as predicted by $p = CV^2/2h$.

Turning our attention to the specific system of Figure 2a, a volume of conducting fluid sits at equilibrium in the channel. The conducting fluid has a Δp that is dominated by a meniscus radius of curvature in the vertical plane R_V that is much smaller than the radius of curvature in the horizontal plane R_H. A row of hydrophobic ($\theta_Y = 180°$) spacer posts is positioned in the channel. In Figure 2b, a voltage is applied, sufficient to advance the conducting fluid forward but not beyond the Laplace barrier created by the row of posts. The conducting fluid is stabilized at the Laplace barrier by the new horizontal radius of curvature R_H imparted by the posts. The Laplace pressure for the advancing meniscus Δp_A that can be imparted by the posts is a maximum when R_H is equal to half the width between the posts ($w/2$), as given by

$$\Delta p_A = \gamma_{ci}(1/R_V + 2/w) \quad (4)$$

Note again that these models are developed without consideration of Gibbs' pinning because of the aforementioned reasons.[6] Now, inserting eqs 2 and 3 into eq 4 allows us to arrive at the general equation for the maximum Laplace pressure imparted by the posts on the advancing meniscus

$$\Delta p_A = \frac{-\left(\gamma_{ci}(\cos\theta_T) + \gamma_{id} + \gamma_{cd} + \frac{1}{2}CV^2\right)}{h} + \frac{2\gamma_{ci}}{w} \quad (5)$$

It can be seen from eq 5 that as the voltage is increased the overall pressure on the advancing meniscus decreases (the first term becomes more negative). With a high enough voltage, the pressure can be decreased to the point that the liquid can wet through the posts. It is also worth noting that the cos θ_T term was not expanded in the equation. This is because the top plate is not an electrowetting plate; however, if the top plate was electrowetting, then eq 3 could also be adapted for cos θ_T .

The calculations can be greatly simplified when considering several additional design features. The top plate carries an In_2O_3/SnO_2 (ITO) ground electrode. The ITO is coated with a hydrophobic fluoropolymer film that is so thin that it is not electrically insulating. With sufficiently low interfacial surface tension between the insulating fluid (oil) and the dielectric (γ_{id}), a Young's angle (θ_Y) of 180° is predicted[13] according to Young's equation: cos $\theta_Y = (\gamma_{id} - \gamma_{cd})/\gamma_{ci}$. Hence, $\theta_T \approx \theta_Y \approx 180°$, and cos $\theta_T \approx -1$.

We must also consider the Laplace pressure at the receding end of the conducting fluid (Δp_R) to calculate the total Δp acting on the fluid. For the receding end, R_H is large and $R_V = h/2$, such that

(12) Jones, T. *J. Micromech. Microeng.* **2005**, *15*, 1184–1187.
(13) Maillard, M.; Legrand, J.; Berge, B. *Langmuir* **2009**, *25*, 6162–6167.

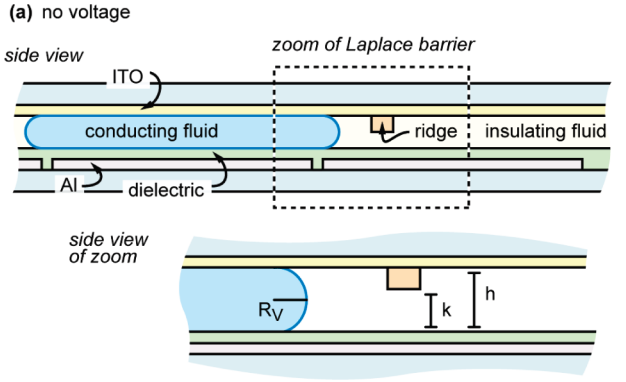


Figure 3. Diagram of a vertical Laplace barrier created by a ridge. All device features are coated with a very thin (50 nm) and hydrophobic fluoropolymer.

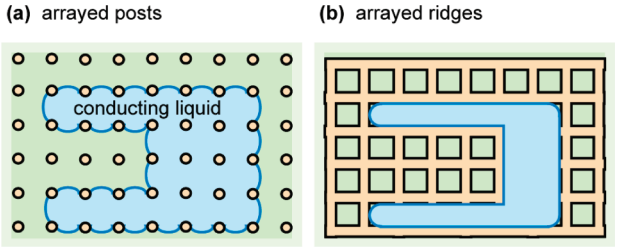


Figure 4. Top view illustrations of arrayed Laplace barriers providing noncircular fluid confinement on the horizontal plane.

in equilibrium the pressures acting on the conducting fluid can be expressed as

$$\Delta p = 0 = \Delta p_R - \Delta p_A \cong \gamma_{ci}(2/h - 1/R_V - 2/w) \quad (6)$$

Now consider an example calculation. For the purpose of simplicity, assume that a voltage is applied to achieve $\theta_B \approx 90°$; therefore, $R_V = h$. From eq 3, it can be solved that $h \cong w/2$ is the limit of stability for Figure 2b. Therefore, if the channel height h was 15 μm, then the spacing between the posts w would be 30 μm. If the applied voltage was increased and correspondingly θ_B decreased, then the conducting fluid could then move past the Laplace barrier (Figure 2c). Once the conducting fluid advances past the Laplace barrier, the voltage can be lowered and the fluid can be advanced using a lower voltage similar to that in a channel with no Laplace barrier. It should be reiterated that the model described immediately above assumes an oil insulating fluid because the discussion and equations are greatly simplified when $\theta_Y \approx 180°$. A more general model was provided in eq 5.

To summarize, the Laplace barrier can provide two unique functions. First, the Laplace barrier provides rectifying fluid flow. A threshold exists for initially advancing through a Laplace barrier but not when receding away from a Laplace barrier. Second, if an array of posts is used, then the fluid can be electrowetted into a geometry that is horizontally noncircular, and the posts can maintain that geometry even after electrowetting stimulus is removed (Figure 4).

Model for the Vertical Laplace Barriers (Ridges)

A second type of Laplace barrier relies on the influence of Laplace pressure in the vertical plane. As shown in Figure 3a, a ridge is patterned on the top substrate with a spacing k between the ridge and the lower substrate. For this case, it can be assumed that R_H is large and that only R_V will influence fluid movement. The Laplace

pressure for the advancing meniscus Δp_A that can be imparted by the ridge is a maximum when R_V is equal to $(k/2)$ and is given by

$$\Delta p_A = 2\gamma_{ci}/k \quad (7)$$

The general form of this equation can be derived similarly to eq 5.

Again, for the sake of simplicity, assume that a voltage is applied such that $\theta_B \approx 90°$ and R_V is doubled to a value of k. At the limit of stability, the pressures acting on the conducting fluid can be expressed as

$$\Delta p = 0 = \Delta p_R - \Delta p_A \cong \gamma_{ci}(2/h - 1/k) \quad (8)$$

It follows that $k = h/2$, and if the channel height h was 15 μm, then k should be 7.5 μm. Again, increasing the voltage to reduce θ_B further would advance the conducting fluid beyond the Laplace barrier.

Note that the ridges were patterned on the top substrate, not the bottom substrate, so as to not locally decrease C in eq 2. Also, when using arrays of ridges in a grid pattern (Figure 4b), the ridges should be horizontally as narrow as possible. Otherwise, the width of the ridges will increase Δp_R, eq 8 will need to be modified, and the Laplace barrier created by the ridges will be weaker.

Experimental Approach

A simple fabrication process was used to create Laplace barriers for testing. First, a glass substrate was sputter-coated with 100 nm Al. Next, ~2 μm of Shipley 1818 photoresist was spin-coated, and the i-line (365 nm) was exposed through a mask with 47.5 mJ/cm^2 total energy. The photoresist was developed using a 5:1 mixture of DI water and a Microposit 351 developer for 45 s. The aluminum was then etched for 3 min using a solution of 120 parts phosphoric acid, 6 parts nitric acid, 6 parts acetic acid, and 6 parts DI water. The photoresist was then stripped, and a patterned electrode formed on the bottom glass plate.

Next, the fabrication process specific to the horizontal Laplace barrier (posts) is described (Figure 2). First, to improve the adhesion of posts, a 1 μm film of MicroChem SU-8 2000 series was spin coated, prebaked (3 min at 95 °C), flood UV-exposed (150 mJ/cm^2), and hard-baked (10 min at 180 °C). Next, to form arrayed posts, a 10 μm SU-8 layer was spin-coated, prebaked, and exposed through a mask, developed with Microchem SU-8 developer for 60 s, and hard-baked. The posts set the channel height (h = 10 μm). Once the post layer was complete, the entire bottom plate was conformally coated with 2 μm of Parylene C dielectric using a Specialty Coating Systems 2010 lab-coater. The bottom plate was then dip-coated in Cytonix Fluoropel 1601 V solution with a 30 s draw time and baked for 30 min at 120 °C to form a hydrophobic fluoropolymer film of ~50 nm thickness and 16 mN/m surface energy. A scanning electron microscope image of the complete bottom plate is pictured in Figure 5a. The top plate for the horizontal Laplace barrier test was prepared from a glass substrate with a transparent ITO electrode and similarly dip-coated with 50 nm of fluoropolymer. For the experiments and voltages used herein, such a thin fluoropolymer is not electrically insulating, and the ITO is conductively accessible at all locations.

The fabrication procedure for the vertical Laplace barrier (ridges) was unique in two aspects (Figure 3). The aluminum electrode was deposited and patterned as previously described. However, on the bottom plate, only a 14 μm SU-8 spacer layer was added around the border of the testing area. This spacer layer overlapped with the outside of the ridges, which were also 14 μm, to create a total channel height of h = 28 μm. The bottom plate was then coated with Parylene C and fluoropolymer. The top ITO-coated plate carried the Laplace barrier, consisting of 14 μm high ridges and another thin fluoropolymer coating. A scanning electron microscope image of the complete top plate is pictured in Figure 5b.

Once the top and bottom plates were fabricated, the fluids needed to be dosed for testing. For ease of visualization, an aqueous

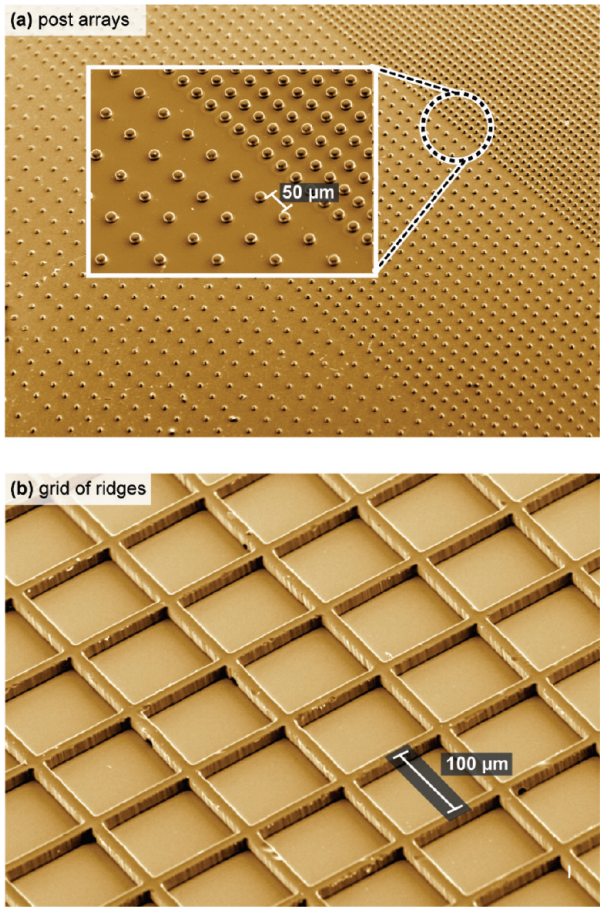


Figure 5. SEM images of (a) horizontal Laplace barriers of arrayed posts with a width and height of 10 μm and pitches varying from 75, to 50, to 25 μm and (b) vertical Laplace barriers of an array of ridges with a ridge width of 25 μm, ridge height of 14 μm, and inter-ridge spacing of 100 μm.

conducting fluid containing 10 wt % red pigment dispersion and a surfactant was custom prepared by Sun Chemical. The pigment dispersion is optically diffuse; therefore, dark-field microscope imaging was implemented (pigment appears bright, Al appears black). This pigment dispersion was pipetted near the Al electrode on the bottom plate. The top and bottom plates were then clamped, and an insulating silicone oil (Dow Corning OS oil) was wicked into the channel between the plates. The interfacial surface tension between the oil and pigment dispersion was $\gamma_{ci} \approx 8.9$ mN/m. Some experiments were also conducted with air (no oil was wicked). Lastly, electrode connections were made to the patterned Al electrode and the top ITO electrode. With oil, the completed devices required ~35 V to modulate the electrowetting contact angle to 90°.

Demonstration of Electrowetting Thresholding

To demonstrate the ability of using a Laplace barrier of posts for thresholding of fluid advancement, an array of posts of decreasing pitch (from w = 200 to 25 μm) was patterned along a strip Al electrode (Figure 5a). First, a test was performed in air, where Young's angle for the pigment dispersion on the fluoropolymer coated surfaces is θ_Y = 81° (Figure 6). The posts are cylindrical, have a smooth surface, and are more widely spaced, such that even in air the expected behavior is determined by Laplace pressure, and Gibbs' pinning[6] can be neglected. To move the dispersion through the w = 75 μm post pitch, an electromechanical pressure of $CV^2/2h$ = 2.65 kN/m^2 was required (Figure 6a). With this pressure held constant, the fluid meniscus moved to the w = 50 μm pitch and

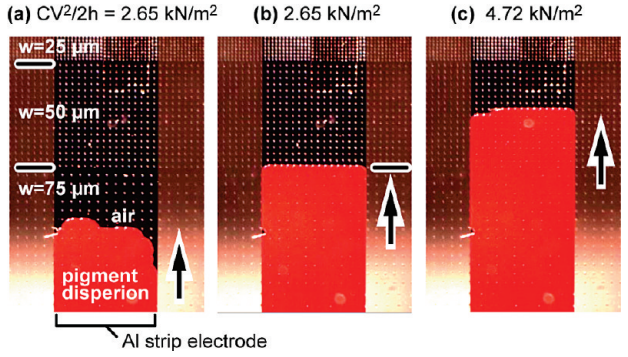


Figure 6. Threshold effect of an arrayed post Laplace barrier in air. Laplace stabilization is confirmed in (b). Dark-field microscope imaging was utilized.

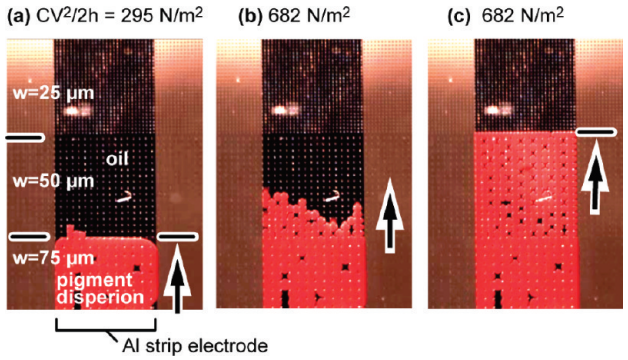


Figure 7. Threshold effect of an arrayed post Laplace barrier in oil. Laplace barrier stabilization is confirmed in (a) and (c). Dark-field microscope imaging was utilized. A supplemental video is available in the Supporting Information.

stabilized there (Figure 6b). To move the fluid through the 50 μm pitch posts, we had to increase the electromechanical pressure to 4.72 kN/m^2 (Figure 6c). This first experiment in air clearly demonstrated the thresholding effect that can be achieved with a horizontal Laplace barrier consisting of arrayed posts. However, for devices tested in air, it is difficult to compare experimental results with the theoretical model because of the very strong influence of contact angle hysteresis and pinning of the receding meniscus at each post. Therefore, the next experiment was conducted in oil.

For an oil system, contact angle hysteresis is less than a few degrees, and the receding end of a meniscus does not pin on posts because $\theta_Y \approx 180°$. In theory, if $\theta_Y > 135°$, then the pigment dispersion will not wick (pin) into the 90° corner that the posts form with the bottom plate. As shown in Figure 7a, the experimentally determined $CV^2/2h$ to move through the $w = 75\,\mu$m posts and stabilize against the $w = 50\,\mu$m post was 295 N/m^2. Equation 6 predicts that the threshold to move through the $w = 75$ and 50 μm posts is 250 and 344 N/m^2. The experimental results shown in Figure 7a therefore fall within this theoretically predicted range. A supplemental video is available in the Supporting Information. In Figure 7a, there is a slight advancement into the $w = 50\,\mu$m posts, but this did not continue further and is likely due to a fabrication defect. As shown in Figure 7b, the electromechanical pressure was increased to 682 N/m^2, and the pigment dispersion moved through the $w = 50\,\mu$m posts. As shown in Figure 7c, at 682 N/m^2, the pigment dispersion stabilized against the $w = 25\,\mu$m posts. This is again in agreement with theory, which predicts that >718 N/m^2 is required to advance the pigment dispersion through the $w = 25\,\mu$m posts.

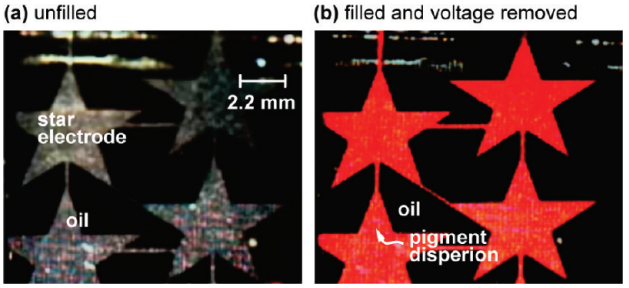


Figure 8. Star electrode filling of an arrayed post device in nonpolar oil: (a) unfilled electrode patterns and (b) filled electrode patterns with voltage removed. Dark-field microscope imaging was utilized.

Not seen in Figure 6 (air) but visually obvious in Figure 7 (oil) is distinct channel or fluid finger formation. These discrete channels eventually remerge but in some instances trap oil. This phenomenon does not impact the threshold pressure of the Laplace barriers; therefore, it will be dealt with separately in a later section (Capillary Fingering and Oil Entrapment).

Demonstration of Virtual Fluid Confinement

Experiments were next performed to validate the virtual confinement of a volume of fluid in a horizontally noncircular shape. A star electrode shape was chosen to inspect the ability of the fluid to both fill and be virtually confined at the sharp corners of the star. In a first experiment, a uniform Laplace barrier of $w = 75\,\mu$m arrayed posts was filled pigment dispersion (Figure 8). The electromechanical pressure for filling the stars was 295 N/m^2, the same as that used in the thresholding tests of Figure 7. As shown in Figure 8, the pigment dispersion filled only those areas above the Al star electrode. When the voltage was removed (Figure 8b), the pigment dispersion remained stabilized in the star geometry. This confirms the ability of a horizontal Laplace barrier (posts) to confine a fluid virtually in a horizontally noncircular geometry. Although not visible at the magnification shown in Figure 8, similar to that observed for Figure 7, discrete channel formation (fingering) and oil entrapment did occur. Therefore, a next experiment was designed to allow the use of oil but eliminate oil entrapment.

The next experiment was performed using the grid of ridges discussed in theory for Figure 3 and pictured in the photograph in Figure 5b. The parameters for the grid of ridges were a channel height $h = 28\,\mu$m, a ridge height of h-$k = 14\,\mu$m, a ridge width of 25 μm, and a spacing in between ridges of 100 μm. This grid formed a vertically oriented Laplace barrier. The theoretically predicted value for the threshold of pigment dispersion advancement is 319 N/m^2. As shown in Figure 9a−g, at an electromechanical pressure of 405 N/m^2, the pigment dispersion was advanced over the star electrode and displaced the oil at a speed of 1.8 mm/s. At this speed, it took ~25 s to fill the first star (Figure 9d). A supplemental video of this pigment dispersion advancement is available in the Supporting Information.

When the voltage was removed (Figure 9h), the ridge Laplace barrier virtually confined the pigment dispersion over the star electrode patterns. Zoom-in photographs were then taken to explore potential discrete channel formation (oil trapping) and to inspect the geometry of virtual confinement. As shown in Figure 10a, no oil entrapment occurred. When the voltage was removed (Figure 10b), the horizontal geometry of the pigment dispersion meniscus conformed to the geometry of the ridge grid. At the point of one arm of the star, the

 DOI: 10.1021/la104090t E

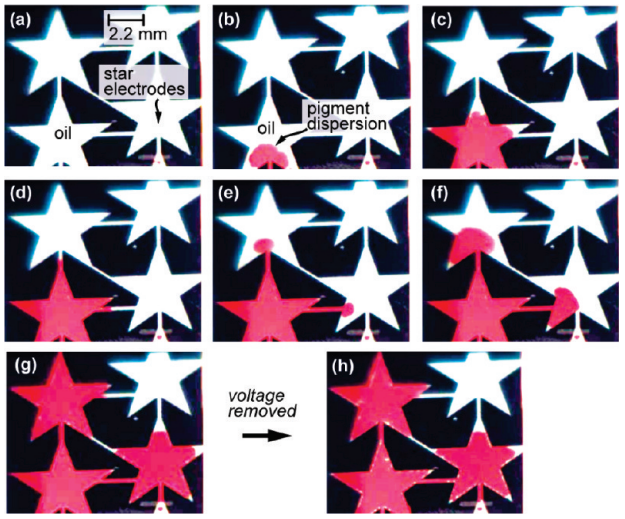


Figure 9. Star electrode filling of an arrayed ridge device in nonpolar oil: (a) unfilled device; (b−g) time lapse of device filling; and (h) voltage removed. A supplemental video is available in the Supporting Information. Light-field microscope imaging was utilized.

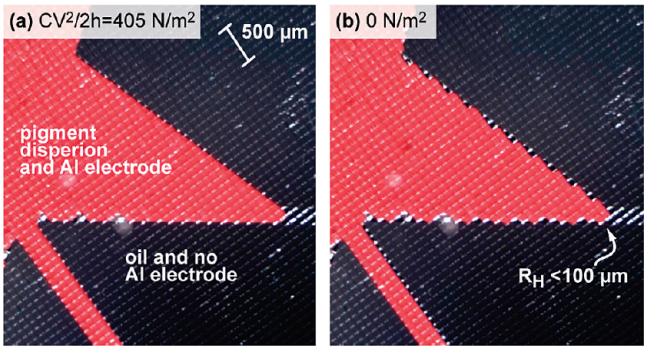


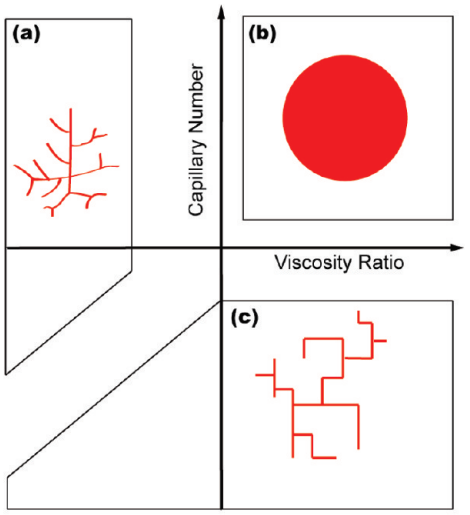
Figure 10. Magnified dark-field microscope image of the star corner in an arrayed ridge device: (a) voltage on and (b) voltage off.

horizontal radius of curvature is clearly $< 100\,\mu$m. Therefore, a grid of ridges is demonstrated as a robust platform for virtual fluid confinement.

Capillary Fingering and Oil Entrapment

As demonstrated herein, when horizontal Laplace barriers (posts) are tested with two fluids (pigment dispersion and oil), fluid finger formation occurs and oil is entrapped. The fluid fingering was not observed when oil was replaced with air. The fluid fingering observed with two fluids is similar to that reported in our previous approach for virtual electrowetting channels.[5] In this present work, more widely spaced posts were observed to exhibit less distinct channels, which is in agreement with our previous work[5] of very closely spaced posts that exhibited very strong fluid fingering (Figure 11d).

To explain finger formation in this and prior work[5] theoretically, we can consider the array of posts as a homogeneously porous media.[14] The fluids in the system are immiscible, and during operation the nonwetting, conductive fluid (pigment dispersion) displaces the wetting, insulating fluid (oil). The displacement of the oil by the nonwetting fluid can be referred to as drainage.[14] There are two parameters critical to understanding the fingering phenomenon: capillary number and viscosity ratio.



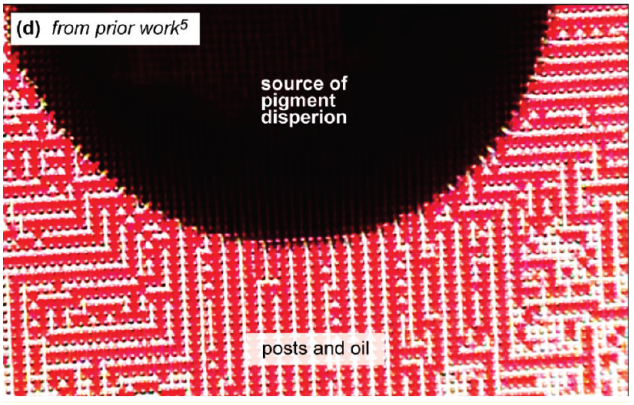


Figure 11. Diagram of drainage domains: (a) viscous fingering domain, (b) stable displacement domain, and (c) capillary fingering domain. The axes are logarithmic. Adapted from Lenormand.[14] Strong capillary fingering from our prior work[5] is shown in (d).

During drainage, the capillary number is defined as the ratio of viscous to capillary forces on the pore scale:

$$C_a = V_c\mu_c/\gamma_{ci} \quad (9)$$

In this equation, V_c is the mean velocity of the conducting fluid, μ_c is the viscosity of the conducting fluid, and γ_{ci} is the interfacial tension between the conducting and insulating fluids.[14] The viscosity ratio between the two immiscible fluids is $M = \mu_c/\mu_i$.

As discussed by Lenormand,[14] and as shown in Figure 11, capillary number and viscosity ratio can be graphically represented as several distinct domains for drainage behavior. For the experiment described in Figure 7, the log of the capillary number is $C_a \approx -4.5$, and the log of the viscosity ratio is $M \approx -0.114$. Although a specific number range is not given on the phase diagram provided by Lenormand, the negative capillary number and near-zero viscosity ratio predicts that the system will be in the capillary fingering domain (Figure 11c). The capillary fingering observed in Figure 7, and in our prior work,[5] is in general agreement with the drainage predicted by Figure 11.

Other experimental results observed for this work are also in agreement with the phase diagram. It was previously noted that capillary fingering does not occur in air (Figure 6). This is expected because Young's angle of the pigment dispersion in air is 81°, which

(14) Lenormand, R. *J. Phys.: Condens. Matter* **1990**, *2*, SA79–SA88.

means that the pigment dispersion is now the wetting fluid (instead of oil). Therefore, the system in air is a situation where a wetting fluid is attempting to displace a nonwetting fluid, which instead is referred to as imbibition. As further described in literature,[14] this system exhibits the behavior of the continuous capillary domain.

Further experiments were performed using the $w = 50$ μm spaced posts in an attempt to eliminate capillary fingering. Figure 11 predicts that a system can move from the capillary fingering domain (Figure 11c) to the stable displacement domain (Figure 11b) if both the capillary number and viscosity ratio are increased. Therefore, in an experiment, we increased the viscosity ratio μ_c by substituting propylene glycol (51.8 cP) for the aqueous pigment dispersion ($\sim$1 cP). We also tested three oils (Dow Corning OS-10, OS-20, and OS-30) of different dynamic viscosities (0.5, 0.8, and 1.3 cP, respectively) to modify the value for μ_i. After propylene glycol was electrowetted into the post field, an image was taken, and the percentage oil entrapment was calculated on the basis of horizontally occupied area. For the OS-30 experiments ($\log M = 1.6$, $\log C_a \approx -3.2$), $28 \pm 1\%$ of the field contained trapped oil. For the OS-20 experiments ($\log M = 1.8$, $\log C_a \approx -3.06$), $19 \pm 1\%$ of the field contained trapped oil. For the OS-10 experiments ($\log M = 2.02$, $\log C_a \approx -2.98$), $15 \pm 1\%$ of the field contained trapped oil. These experiments clearly show that increased viscosity ratio and capillary number results in less oil entrapment. However, these experiments show that the system is still in the capillary fingering domain (Figure 11c). To exit this domain, the capillary number would likely need to be improved to impractical values. Therefore, it is our present understanding that some degree of capillary fingering will always occur when electrowetting through posts in the presence of oil.

Up to this point in the discussion, we have only considered a fixed post pitch (w). The capillary number becomes multiplied by a factor of a^2/κ when taking different pore sizes into consideration,[15] where a is the pore radius and κ is the intrinsic permeability. It is possible to increase the capillary number and decrease capillary fingering by increasing the post pitch (w). This is also in agreement with experiment because more widely spaced posts were observed to exhibit less fingering in this and previous work.[5] However, using very wide post pitch is impractical because the influence of the horizontal Laplace barriers is also diminished.

The use of ridges (vertical Laplace barriers) exhibits no capillary fingering because they are only semiporous and work by constricting the flow into thin gaps instead of diverging the flow around a structure. This system is very similar to that of two-phase displacement in Hele-Shaw cells, where small local instabilities in the flow are dampened out by the advancing meniscus before significant fingering occurs.[16]

Further Discussion and Applications

We have demonstrated herein a second generation approach for stabilizing fluids after manipulation by electrowetting. The Laplace barriers described herein have not been optimized for maximum speed, minimum or maximum fluid dimensions, or other factors that may be useful from an applications viewpoint. Not reported herein, but under development, is a new design for Laplace barriers that utilizes short posts that do not span the channel height and would therefore combine the function of posts and ridges. Results concerning this design will be reported in a future publication.

Even though the Laplace barriers have not been fully optimized, the functionality provided by Laplace barriers is now sufficiently understood to speculate on several applications. A first application is lab-on-chip, as previously described[5] for our first-generation platform of arrayed electrowetting posts. For lab-on-chip, Laplace barriers provide unification of programmable electrowetting control and the possibility of continuous channel function.

A second application is changing the geometry of colored fluids for display devices. The demonstration shown herein already proves that with multiple electrodes simple reconfigurable character or symbol display is possible. A key feature provided by the Laplace barriers is that such a device can consume zero electrical power after a fluid geometry is selected. Furthermore, the Laplace barriers made of ridges allow the display of colored fluids with no pixel borders and none of the optical losses associated with pixel borders. The top plate also does not need to be a continuous sheet of ITO, just a narrow strip or grid forming a ground electrode. Therefore, the optical performance of such a display device should reach the theoretical limit for color saturation and brightness; displaying a diffuse and saturated color pigment dispersion right against the surface of a transparent front plate.

Laplace barriers also provide significant value for passive-matrix electrowetting control.[9] Passive matrix control of electrowetting imparts a voltage along the entire length of row or column electrode. This voltage can still be significant enough to cause electrowetting motion of fluid. The Laplace barriers described herein can be used to prevent the motion of fluid except at a selected row/column intersection because at all other locations the electromechanical pressure would be below the threshold pressure for the Laplace barrier. Laplace barriers can also be useful inside an individual electrowetting display device[7,17] by providing repeatable grayscale reset states. Lastly, consider placing two or more distinct fluids adjacent together in an open microchannel. A tight packing density is not possible because of the circular horizontal geometry of the fluids. Laplace barriers can act as a separating barrier between closely spaced fluids with tight packing density and without the risk of merging of the two or more tightly packed fluids.

Acknowledgment. We acknowledge partial support from NSF Career award no. 0640964 (University of Cincinnati), NSF CBET award no. 0729250, NSF IHCS award no. 1001141, NSF IGERT award no. 0333377, AFRL contract no. 5408-25-SC-0003 (Rajesh Naik), and an ARL grant no. W9111NF-09-2-0034 (Dave Morton and Eric Forsythe).

Supporting Information Available: Supplemental videos of the threshold effect of an arrayed post Laplace barrier in oil and the star electrode filling of an arrayed ridge device in nonpolar oil. This material is available free of charge via the Internet at http://pubs.acs.org.

(15) Chau, J. F.; Or, D. *Phys. Rev. E* **2006**, *74*, 056304/1–056304/11.
(16) Park, C. W.; Homsey, G. M. *J. Fluid Mech.* **1984**, *139*, 291–308.
(17) Yang, S.; Zhou, K.; Kreit, E.; Heikenfeld, J. *Appl. Phys. Lett.* **2010**, *97*, 143501/1–143501/3.